Journal of Cleaner Production 218 (2019) 192–201

Contents lists available at ScienceDirect

Journal of Cleaner Production

journal homepage: www.elsevier.com/locate/jclepro

Complex utilisation of ekibastuz brown coal fly ash: Iron & carbon separation and aluminum extraction

D. Valeev [a, *], I. Kunilova [b], A. Alpatov [c], A. Mikhailova [d], M. Goldberg [e], A. Kondratiev [f]

[a] I.P. Bardin Laboratory for Problems of Metallurgy of Complex Ores, Baikov Institute of Metallurgy and Materials Science, Russian Academy of Science, 119334, Leninsky prosp., 49, Moscow, Russia
[b] Laboratory № 4.2. Complex processing of non-traditional mineral materials, Research Institute of Comprehensive Exploitation of Mineral Resources—IPKON, Russian Academy of Sciences, 111020, Kryukovskii tupik 4, Moscow, Russia
[c] Laboratory of Material Diagnostics, Baikov Institute of Metallurgy and Materials Science, Russian Academy of Science, 119334, Leninsky prosp., 49, Moscow, Russia
[d] Laboratory of Crystal Structure Studies, Baikov Institute of Metallurgy and Materials Science, Russian Academy of Science, 119334, Leninsky prosp., 49, Moscow, Russia
[e] Laboratory of Ceramic Composite Materials, Baikov Institute of Metallurgy and Materials Science, Russian Academy of Science, 119334, Leninsky prosp., 49, Moscow, Russia
[f] Scientific Research Centre "Thermochemistry of Materials", National University of Science & Technology "MISIS", 119991, Leninsky prosp., 4, Moscow, Russia

ARTICLE INFO

Article history:
Received 27 November 2018
Received in revised form
30 January 2019
Accepted 31 January 2019
Available online 1 February 2019

Keywords:
Coal fly ash
Magnetic separation
Flotation
Autoclave acid leaching
Aluminum extraction
Fly ash treatment

ABSTRACT

Fly ash landfills that accumulate a by-product of coal combustion and gasification represent a permanent threat to the surrounding environment due to many factors (air and water pollution, soil contamination, wildlife poisoning, etc). Moreover, disposed coal fly ash may contain significant amounts of valuable elements that are not extracted and potentially wasted. To improve the above situation, a combined ash treatment process was developed for utilisation of the coal fly ash waste from coal-fired power stations. The ash treatment includes three stages: 1) magnetic separation of an iron-containing fraction, 2) carbon separation by floatation, and 3) extraction of aluminum by the autoclave hydrochloric acid leaching. The lab-scale results of the ash treatment applied to the Ekibastuz brown coal fly ash from the Omsk power stations (Russia) were presented and discussed. The XRD analysis showed that the fly ash consists primarily of quartz, mullite and magnetite. It was found that the magnetic fraction separated at the first stage is enriched in magnetite (over 20 wt %), the carbon content in the concentrate after flotation increases to 27 wt %, and 90–95% of aluminum can be extracted during the autoclave acid leaching. The SEM analysis showed that the magnetite phase is grown on the surface of alumosilicate spheres as ~1 μm cubic crystals. The effect of the autoclave temperature and exposure time on the Al extraction efficiency was also investigated and analysed in the present paper. The optimal autoclave temperature and exposure time were found to achieve the maximum Al extraction efficiency. It was also found by the SEM microanalysis that further extraction of aluminum is not economically feasible since the remaining Al is evenly surrounded by SiO_2 in the fly ash particles.

1. Introduction

A lot of power stations world-wide still use coal combustion as a main process to generate electricity and heat. In the city of Omsk (second largest city in Siberian region of Russia) thermal power stations utilise brown coal from the Ekibastuz coal field (Kazakhstan), which is characterised by high ash content (up to 40%) (Dikhanbaev et al., 2018). Electricity and heat for the Omsk city is produced mainly by two coal-fired power stations TPS-4 and TPS-5 that generate 450 000 and 1 150 000 tons of coal fly ash (CFA) per year, respectively. In total, ash disposal sites near Omsk accumulate more than 75 million tons of CFA up to 2017 (Sirotyuk and Lunev, 2017).

Ash disposal in landfills is not economically and ecologically sustainable, because ash contains a lot of valuable as well as potentially toxic elements. Also, in Siberian region, ash landfills

* Corresponding author.
E-mail addresses: dvaleev@imet.ac.ru (D. Valeev), ecoreagent@yandex.ru (I. Kunilova), avalpatov@imet.ac.ru (A. Alpatov), amikhailov@imet.ac.ru (A. Mikhailova), mgoldberg@imet.ac.ru (M. Goldberg), al.v.kondratiev@gmail.com (A. Kondratiev).

https://doi.org/10.1016/j.jclepro.2019.01.342
0959-6526/

should be watered in summers to prevent wind erosion, dammed from rivers and lakes to avoid high water in springs, and isolated from groundwater to avoid leaching and infiltration of harmful elements such as As, Se, Pb, etc (Flues et al., 2013). Noncompliance of these precautions could result in disastrous consequences: water and soil contamination (Dandautiya et al., 2018), animals poisoning and health impact (Ruhl et al., 2009). For example, mechanical (wind) erosion of dry ash landfills in summers leads to air pollution, which may cause serious health problems (Schins and Borm, 1999). It must be mentioned that one of the ash landfills of Omsk TPS-4 is located near the Irtysh River, a major river and main water source in the region. Its water may be polluted if annual spring flood destroys the dam, which in turn could result in a huge environmental impact in the Irtysh itself and adjacent rivers. Therefore, a new method of CFA recycling or/and utilisation is highly demanded, especially in this region.

CFA usually contains 20 to 35 wt % of Al_2O_3, which can partially be extracted by different methods (Ding et al., 2017; Sahoo et al., 2016). Alkaline treatment of fly ash includes in general two stages: first, low-concentration alkaline leaching of SiO_2 (desilication); second, leaching of aluminum (Liu et al., 2014; Wang et al., 2014). The extent of SiO_2 extraction can vary from 30 to 65% (Jiang et al., 2015; Lu et al., 2017). Mixing of fly ash and sodium carbonate (Na_2CO_3) with further sintering can be used to intensify the extraction process (Gong et al., 2016; Guo et al., 2014). Another method to increase the Al extraction is to add slaked lime ($Ca(OH)_2$) for bonding SiO_2 into sodium calcium hydrosilicate - ($NaCaHSiO_4$), which does not react with alkali (NaOH) (Li et al., 2014; Sun et al., 2016). The extent of the Al extraction can reach 95% with the use of the abovementioned methods (Ding et al., 2016).

There are ash utilization methods that do not require prior removal of SiO_2. Sintering of mullite and Na_2CO_3 or calcium carbonate ($CaCO_3$) occurs on annealing at 700–900 °C (Liu et al., 2018; Yan et al., 2018). To reduce the annealing temperature and time, it is possible to use microwave heating of the mixture (Liu et al., 2016; Tanvar et al., 2018; Zhang et al., 2015). Sintering with ammonia sulphate ($(NH_4)_2SO_4$) at 400 °C and subsequent leaching of the sinters enables to extract up to 95% of aluminum. (Sun et al., 2017; van der Merwe et al., 2017). However, besides Al, other metals (Ca, Mg and Ti) can also go into the solution (Doucet et al., 2016).

Sulphuric acid leaching of fly ash is commonly conducted in two stages: preliminary dissolution of aluminum from fly ash, and subsequent H_2SO_4 leaching of the solid residue sintered after filtration with lime or Na_2CO_3. This approach can extract up to 95% of aluminum (Sangita et al., 2017; Wei et al., 2018).

Recent studies (e.g. S. Li et al., 2017) on the Al extraction from CFA using acid leaching show that hydrochloric acid is the most reactive in regard to Al compared to sulphuric, nitric and hydrofluoric acids. If lithium is present in fly ash, up to 75–80% of it goes into solution (Hu et al., 2018). However, if leaching is carried out at atmospheric pressure (e.g. 6M HCl, T = 107 °C) the extent of Al extraction does not exceed 70% (Luo et al., 2013; Singh et al., 2015; Valeev et al., 2018). One of the most perspective methods to intensify leaching of a high-silica aluminum-containing feedstock is to use autoclaves (Lin et al., 2018; Wu et al., 2012, 2014; Xiao et al., 2018). This method allows to exclude preliminary annealing and two-stage leaching. As silicon dioxide does not react with acids a preliminary desilication is not necessary. Besides aluminum iron will also go into the solution, which makes it necessary first to remove magnetite by magnetic separation.

Aluminum is mainly present in fly ash as mullite. A reaction between mullite and hydrochloric acid (6M) at a boiling temperature results in extraction of maximum 15% of aluminum. Fluorides of alkali and alkaline earth metals (KF, NaF, CaF_2) as well as ammonium fluoride (NH_4F) are usually added to intensify the Al extraction. A fluoride reacts with SiO_2 and destroys the Si–Al bond, forming SiF_4, which hydrolyses with formation of H_2SiF_6 (Li et al., 2011). This method leads to a substantial increase of the Al extraction efficiency, up to 90–95% (Tripathy et al., 2015). However, hydrofluoric acid can form during such treatment, which prevents aluminum chloride solution to be readily used as a coagulant for water purification (Cheng et al., 2012; Hu et al., 2017; Yan et al., 2016).

In the present work a combined treatment of the raw CFA collected from the Omsk TPS-4 was carried out in three stages: 1) iron separation by magnetic separation, 2) carbon separation by flotation, and 3) aluminum extraction by autoclave acid leaching. During this treatment first the magnetic and non-magnetic fractions were separated from the initial CFA; then the C-containing fraction was separated from the non-magnetic fraction; and finally the remaining material was processed to extract Al into the aluminum chloride solution. The effects of the autoclave temperature and exposure time on the Al extraction efficiency were investigated and analysed.

2. Materials and methods

2.1. Raw materials

The raw CFA collected from the Omsk TPS-4 ash disposal site (that contains ~37 million tons of fly ash) was used as an initial waste material. The CFA is produced from combustion of the Ekibastuz brown coal (Kazakhstan) on the Omsk TPS-4. The average chemical composition of the raw CFA is given in Table 1. The XRD analysis of the raw CFA is provided in Section 3.1 (see Fig. 3). Also, the results of microstructure analysis by SEM are reported in Sections 3.1, 3.2 and 3.4.

Other raw materials used in the present study include: hydrochloric acid of the reagent grade (LLC “Component-Reaktiv”, Russia); kerosene KO-25 (LLC “Componet-Reaktiv”, Russia); methylisobutylcarbinol ($C_6H_{14}O$), CAS no. 108-11-2, (Merck, Russia).

2.2. Methods

A flow chart of the CFA treatment process is shown in Fig. 1. In total, it includes the wet magnetic separation, grinding, screening, flotation, autoclave leaching and filtration. It can be seen that four different output materials are produced at different stages: the Fe-enriched magnetic fraction, C-enriched fraction, Al chloride solution, and solid residue.

2.3. Measurement and characterisation

The X-ray diffraction (XRD) analysis of initial CFA and samples

Table 1
The average chemical composition [wt. %] of CFA from TPS-4 (Omsk, Russia).

Component	SiO_2	Al_2O_3	Fe_2O_3	TiO_2	K_2O	CaO	MgO	MnO	Na_2O	P_2O_5	LOI[a]
Contents	59.66	24.26	5.42	1.15	0.74	0.88	0.40	0.11	0.44	0.45	6.49

[a] LOI – loss on ignition.

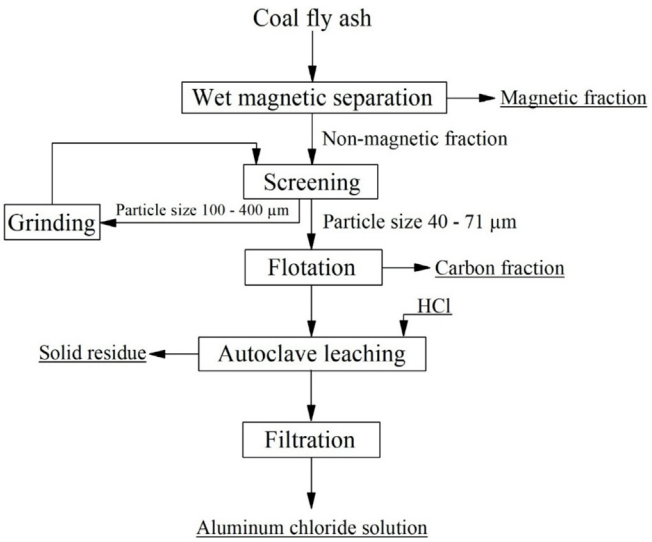

Fig. 1. A flow chart of the combined ash treatment.

after magnetic separation was carried out in a range of 2θ from 9° to 100° with a step of 0.02° using a diffractometer Ultima IV, (Rigaku, Japan) with a Cu-Kα radiation source. The applied voltage and current was 40 kV and 30 mA, respectively. Silica gel was added (about 20 wt %) in the samples to reduce preferential texture (grain) orientation. Determination of quantitative and qualitative sample compositions was done by a software programme PDXL (Rigaku).

The carbon and sulphur contents were determined by a fractional gas analyser CS-600 (LECO Corporation, USA). Samples (~1 g) were placed in ceramic crucibles and then loaded into an induction furnace. The C and S concentrations were determined by infrared absorption of gaseous CO_2 and SO_2 during sample combustion in oxygen atmosphere.

Analysis of surface morphology, microstructure and elemental composition of fly ash was carried out using a scanning electron microscope Vega II (Tescan, Czech Republic) and light microscope LEO 1420 (Carl Zeiss, Germany).

The chemical analysis of solid and liquid samples was carried out using an atomic emission spectrometer with inductively coupled plasma ICAP 6300 DUO (Thermo Scientific, USA).

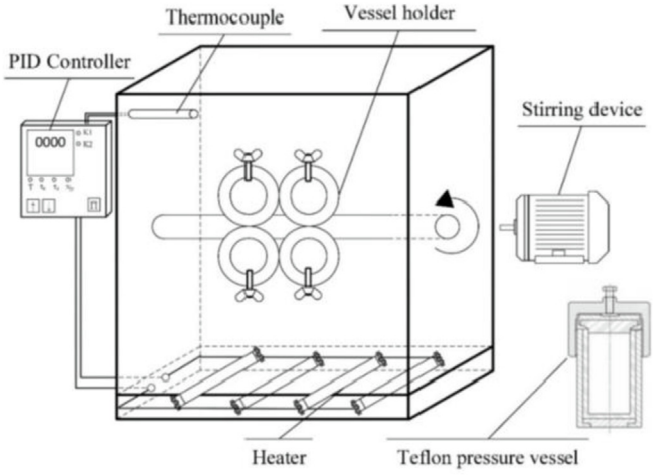

Fig. 2. Schematic of the experimental set-up for autoclave acid leaching.

2.4. Magnetic separation

A roll-type magnetic separator MBS 150 × 125 (NPO "Erga", Russia) was used to separate the magnetic and non-magnetic fractions of CFA. Initial CFA samples of ~500 g were mixed with water and loaded into the separator. The magnetic field strength applied was 110 mT.

2.5. Flotation tests

Carbon flotation tests were carried out in a flotation machine 189FL (REC "Mekhanobr-Tekhnika", Russia) using methyl isobutyl carbinol (MIBC) as a foamer (frother) and kerosene KO-25 as a collector. Typical amount of non-magnetic fractions and water volume were 20 g and 100 ml, respectively.

The particle size for flotation was selected to be of 40–71 μm (see Section 3.2). A planetary mill Pulverisette 7 (Fritsch, Germany) was used to grind a large-size fly ash fraction.

Preparation of the collector water emulsion was carried out as follows: 6.4 ml of kerosene ($\rho = 0.781$ g/cm^3) was placed in a 50 ml flask, topped up with distilled water, and mixed up thoroughly by ultrasound for 5 min using an ultrasound bath Sonorex Digitec (Bandelin Electronic, Germany). The kerosene concentration was 100 g/l and the volume of the emulsion added to the pulp was 0.5; 1.0; 1.5; 2.0, 2.5, 5.0, 7.5 ml.

Preparation of the frother was carried out as follows: 0.93 ml of MIBC ($\rho = 0.806$ g/cm^3) was placed in a 50 ml flask and topped up with distilled water. The volume of the frother added to the pulp was 1.8 ml, while the MIBC concentration in water during flotation was 0.33 g/l.

Flotation tests were carried out as follows: non-magnetic

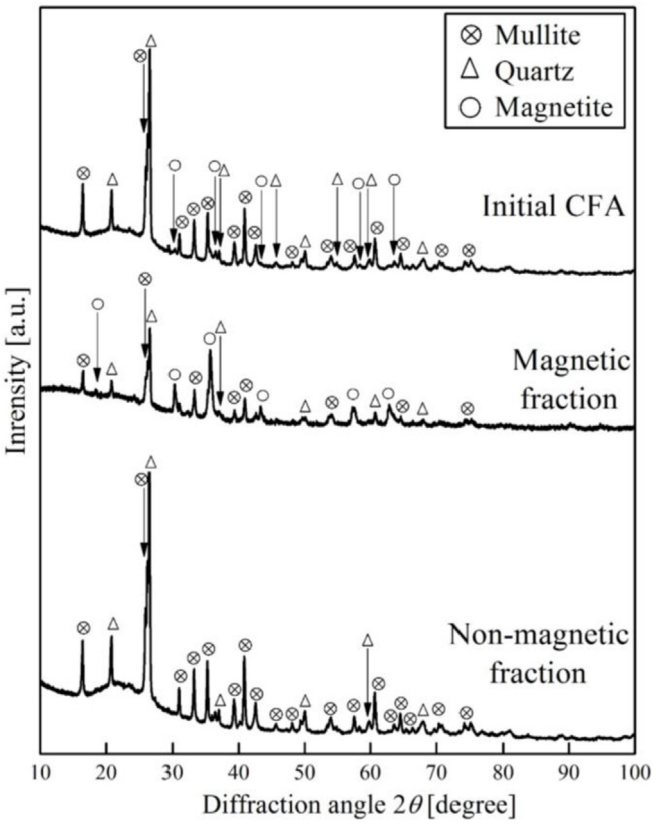

Fig. 3. XRD patterns of the initial CFA and the magnetic & non-magnetic fractions after the wet magnetic separation.

Table 2
The bulk chemical composition [wt. %] of the magnetic & non-magnetic fractions after the wet magnetic separation of CFA from TPS-4, Omsk, Russia.

Component	SiO_2	Al_2O_3	Fe_2O_3	TiO_2	K_2O	CaO	MgO	MnO	Na_2O	P_2O_5	LOI[a]
Magnetic fraction	55.94	14.73	20.2	0.75	0.4	1.28	0.66	0.67	0.28	0.64	4.45
Non-magnetic fraction	62.89	27.01	0.63	1.33	0.35	0.09	0.14	0.18	0.32	0.42	6.77

[a] LOI – loss on ignition.

fractions and water were loaded into a flotation chamber, mixed up for 3 min, then mixed with calcium hydroxide for 2 min to obtain pH = 11, then mixed with the collector for 1 min, mixed with the frother for 1 min and finally floated until the froth mineralisation stops (~1.5 min).

Flotation tailings and the carbon concentrate were first dried at T = 60 °C for 24 h, then weighed to determine the product output, and finally the carbon and sulphur content was analysed as described in Section 2.3.

The following flotation efficiency index commonly used in mineral processing (Vasilyev and Kuskov, 2018) was employed as an efficiency criterion:

$$E = [(\varepsilon\text{-}\gamma) / (100 - \alpha)] \times \cdot 100\% \quad (1)$$

where ε is the percentage of carbon extraction from the non-magnetic fraction; γ is the amount of the carbon concentrate relative to the initial mass of the non-magnetic fraction; α is the carbon content in the CFA non-magnetic fraction.

2.6. Extraction of aluminum

Leaching of fly ash by hydrochloric acid to extract aluminum was carried out in a laboratory home-made autoclave (Fig. 2) using stainless steel capsules with 50 ml Teflon inserts (Deschem, China). The autoclave temperature was governed by a PID controller with ±1 °C accuracy. The heating time from room temperature up to a particular temperature was approximately 1 h. The exposure times at different temperatures (170, 180, 190, 200 °C) were 1, 2, 3, 4 h, respectively. The HCl concentration was 345 g/l (30%); the ratio S:L = 1:5. The efficiency of aluminum extraction was calculated by the following formula:

$$\eta = [Al_1 / Al_2] \times \cdot 100\% \quad (2)$$

where $Al_{1,2}$ are the aluminum concentrations after and before leaching, respectively.

3. Results and discussion

3.1. Wet magnetic separation

Fig. 3 showed the XRD results for the initial CFA (TPS-4, Omsk, Russia), and for the magnetic & non-magnetic fractions after the wet magnetic separation. It can be seen that the initial CFA consists mainly of mullite, quartz and magnetite. In general, the mullite phase is a non-stoichiometric solid solution between SiO_2 and Al_2O_3 with an approximate formula $Al_6Si_2O_{13}$. The quartz and magnetite phases have stoichiometric formulae SiO_2 and Fe_3O_4, respectively; however, while quartz is a SiO_2 polymorph, magnetite generally represents a solid solution between FeO and Fe_2O_3 with a spinel-type structure that can accommodate other atoms like Ca, Mg and Mn.

The wet magnetic separation tests demonstrate that the magnetic fraction can consist up to 10% of the initial fly ash mass. The magnetite content in the magnetic fraction after separation increases from 5 to 20 wt %. The non-magnetic fraction contains less than 1 wt % of iron oxide, and the Al_2O_3 amount increases from 24 to 27 wt % (Table 2). It can be seen that Ca, Mg, Mn, P occur mainly in the magnetic fraction, while Ti and C are present in the non-magnetic fraction. A possible reason for such element separation is that Ca, Mg and Mn apparently occur in the magnetite phase, while Ti may be associated with the quartz phase and carbon occurs mostly in a free form, as demonstrated in Section 3.2. It can also be seen that significant amounts of SiO_2 and Al_2O_3 are present in the magnetic fraction, which indicates incomplete separation of magnetite from quartz or/and mullite (see SEM results below).

Morphology of ash particles from the magnetic and non-magnetic fractions obtained by SEM is shown in Fig. 4(a and b), while the corresponding elemental spectra are given in Table 3. The magnetic fraction consists primarily of spherical particles of 30–60 μm, with small cubic crystals (about 1 μm) of magnetite grown on their surface (see Fig. 5(a and b)) as reported also by other researchers (J. Li et al., 2017; Valentim et al., 2018). The amount of magnetite on the particles surface is not significant compared to the alumosilicate content, which implies that the magnetite concentration in the magnetic fraction cannot be increased to 50–75%. Li and co-workers showed (G. Li et al., 2014) that reductive roasting of the magnetic fraction with sulphates or carbonates of alkali metals can produce iron grains with size up to 50 μm, which can further be separated from the alumosilicate particles by magnetic separation. The non-magnetic fraction consists of agglomerates of irregular shape with a size of 20–80 μm (see Fig. 5(c and d)).

Thus, it was found that the magnetite amount in the magnetic

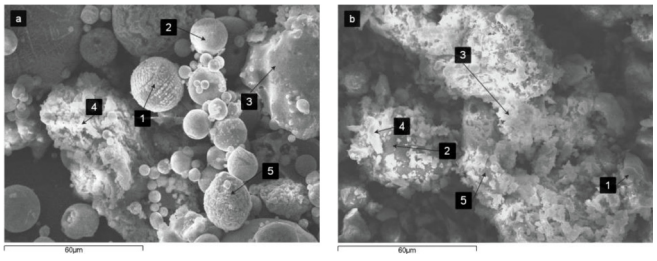

Fig. 4. Typical SEM images of the (a) magnetic and (b) non-magnetic fractions.

Table 3
The elemental compositions [wt. %] of particles from the magnetic and non-magnetic fractions (see Fig. 4 for the spectra numbers).

Spectrum	O	Na	Mg	Al	Si	Ca	Ti	Fe
Magnetic fraction								
1	69.40	–	1.47	1.04	5.72	0.62	–	21.75
2	65.53	–	–	0.55	1.17	0.70	–	32.05
3	50.92	–	–	–	10.29	–	–	38.79
4	75.07	–	0.20	3.71	19.8	–	–	1.22
5	63.52	–	1.82	1.90	3.80	0.53	–	28.43
Non-magnetic fraction								
1	72.99	–	–	8.97	15.98	0.57	0.37	1.11
2	63.35	–	1.05	4.34	20.21	2.79	6.30	1.96
3	74.16	–	–	5.02	20.82	–	–	–
4	74.35	0.27	0.43	10.80	13.54	0.35	–	0.27
5	59.77	–	–	17.35	22.88	–	–	–

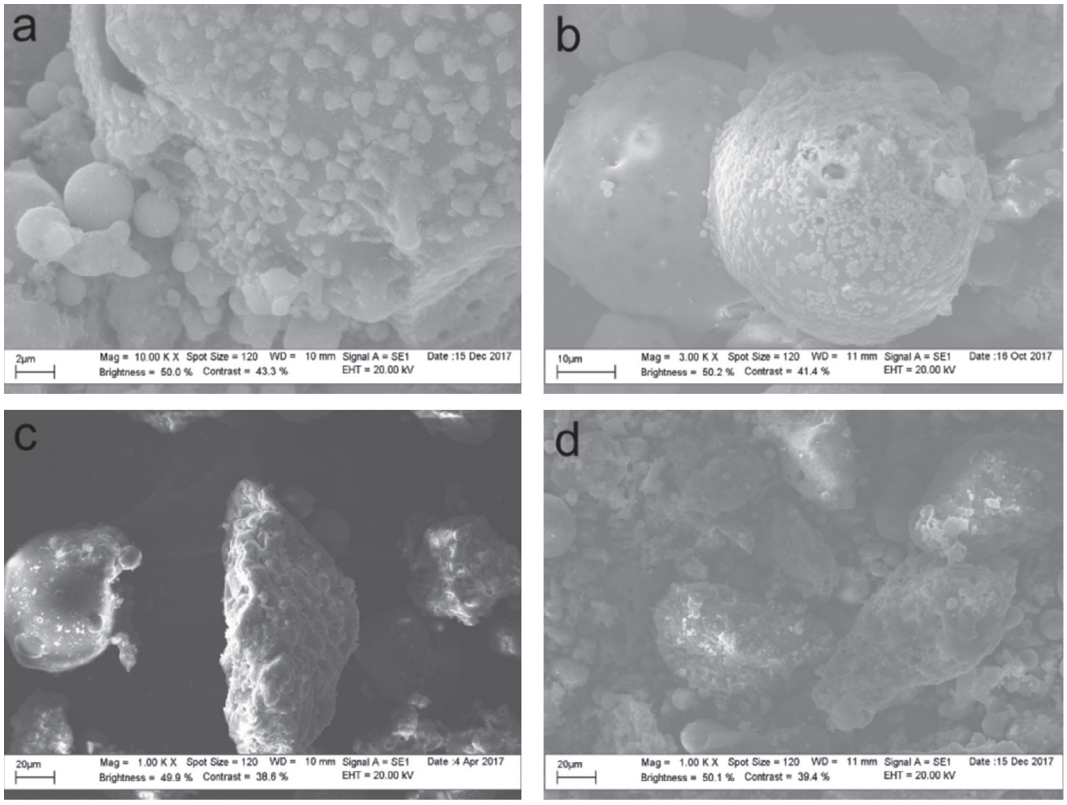

Fig. 5. The enlarged SEM images of CFA particles from the (a–b) magnetic fraction and (c–d) non-magnetic fraction.

Table 4
The carbon and sulphur concentrations in the non-magnetic fraction as a function of the particle size.

Particle size, μm	Fraction in CFA, %	Carbon content, wt. %	Sulphur content, wt. %
315–400	0.28	30.9	0.242
200–315	1.65	25.6	0.179
160–200	1.78	18.5	0.128
100–160	17.88	9.96	0.069
71–100	15.46	7.14	0.053
63–71	19.33	5.57	0.041
40–63	18.59	3.72	0.029
40 <	25.02	2.27	0.023

fraction after separation increases from 5.3 to 20.2 wt %, while the Al_2O_3 amount in the non-magnetic fraction increases from 24.5 to 27 wt %. Further increase of the magnetite fraction is not possible due to a small size (~1 μm) of its crystals located on the alumosilicate spheres.

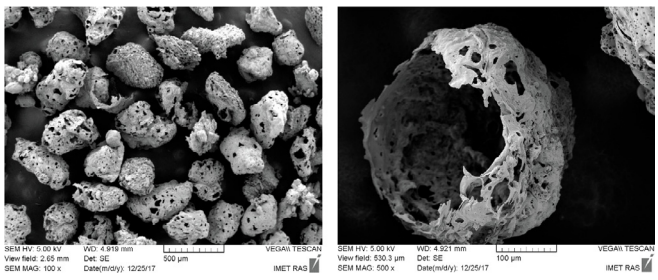

Fig. 6. The SEM images of carbon particles from the CFA non-magnetic fraction.

3.2. Carbon flotation

The non-magnetic fraction obtained after the wet magnetic separation contains about 6.5 wt % of carbon and 0.04 wt % of sulphur. It was screened into size fractions from 40 to 400 μm, and the C and S concentrations was determined for each size fraction (Table 4).

It can be seen from Table 4 that fly ash particles over 100 μm contain 10-30 wt % of carbon and 0.07–0.24 wt % of sulphur. Fly ash particle size distribution and carbon content agree with the reported data by Bartoňová (2015). Fig. 6 shows porous spherical particles that contain most carbon present in fly ash (Hower et al., 2017). It can be seen that the average size of those particles is bigger than 200 μm.

It was found (Yang et al., 2018) that the most suitable particle size for flotation should lie in a range of 40–71 μm Carbon flotability depends on the pH index, so that with increasing pH the carbon output into the concentrate increases (Ryabov et al., 2018); thereby pH = 11 was selected in the present work. The ash fraction

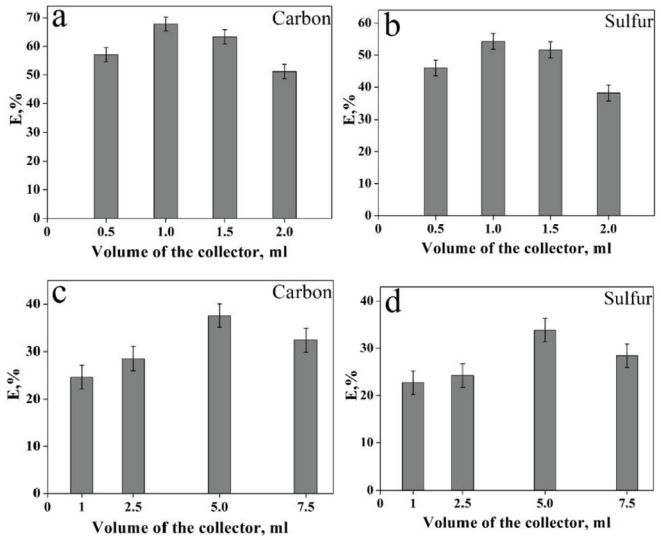

Fig. 7. The effect of the collector volume on the flotation efficiency index *E*: (a–b) for CFA particles of 40–71 μm after screening non-magnetic fraction carbon; (c–d) for CFA particles of 100–400 μm after grinding to 40–71 μm.

that contains particles over 71 μm was subjected to grinding and was further processed by flotation. Kerosene was chosen as the collector in flotation due to its effectiveness and cheap price (Han et al., 2018; Ryabov et al., 2016). The results of flotation tests are shown in Fig. 7(a–d), which represent the efficiency index *E* (calculated by Equation (1) for carbon and sulphur) as a function of the collector volume for (a-b) small particles (40–71 μm) processed by flotation and (c-d) large particles (100–400 μm) first grinded to 40–71 μm and then processed by flotation. It can be seen that the efficiency index for carbon increases to ~67.8% as the collector volume changed from 0.5 to 1.5 ml. Further increase of the collector volume to 2 ml decreases the *E* index to 51% (Fig. 7a). As the large-size (100–400 μm) ash fraction contains significantly more carbon than the small-size fraction (<100 μm), the collector volume was increased; the best efficiency was achieved on adding 5 ml of kerosene (Fig. 7(c)). However, as in the case of small-size fraction, an increase of the collector volume to 7.5 ml decreases the flotation efficiency index to 32%, because the larger the collector volume, the greater the amount of alumosilicate particles collected in flotation. It can be seen from Fig. 7(b, d) that similar trends were observed for sulphur flotation, but poorer flotation efficiency indices can be achieved than those for carbon (the corresponding values are 54 and 33.8%).

Fig. 8 shows micrographs of the carbons fraction after flotation. The carbon particles are present as ~50 μm porous spherules (Fig. 8(a and b)) and as dense elongated structures of 80–100 μm with rounded holes of 1–5 μm diameter (Fig. 8(c and d)). The maximum carbon content that can be achieved in the concentrate after flotation was 18 wt % with processing only small particles and 26.9 wt % with grinding large particles and processing both large and small particles.

Thus, it was found that the carbon content in the concentrate after flotation with kerosene as the collector increases from 6.5 to 27 wt %. The flotation efficiency index can reach almost 68% for carbon and 54% for sulphur.

3.3. Autoclave leaching by hydrochloric acid

The XRD analysis of the non-magnetic fraction showed only the presence of quartz and mullite (see Fig. 3). Mullite is the only phase that contains aluminum, so the Al extraction process (leaching by hydrochloric acid) can roughly be represented by the following reaction:

$$3Al_2O_3 \cdot 2SiO_{2(s)} + 18HCl_{(l)} = 6AlCl_{3(aq)} + 2SiO_{2(s)} + 9H_2O_{(l)} \quad (3)$$

The effect of the autoclave temperature and exposure time on the Al extraction efficiency is shown in Fig. 9. It can be seen that an increase of the autoclave temperature leads to an increase of the Al extraction efficiency. The higher extraction efficiency of 90–95% was observed at temperatures 190–200 °C after ~3 h of leaching. The chemical composition of the solution obtained at T = 200 °C and τ = 3 h is as follows [g/l]: Al – 23.6, Fe – 2.1, K – 0.9, Mg – 0.3, Na – 0.6, Ti – 0.6, Sc – 0.002. A further increase of the Al extraction efficiency with increasing temperature is believed to be possible, but it may lead to rapid chemical corrosion of the equipment due to much higher aggressiveness of HCl at temperatures above 200 °C.

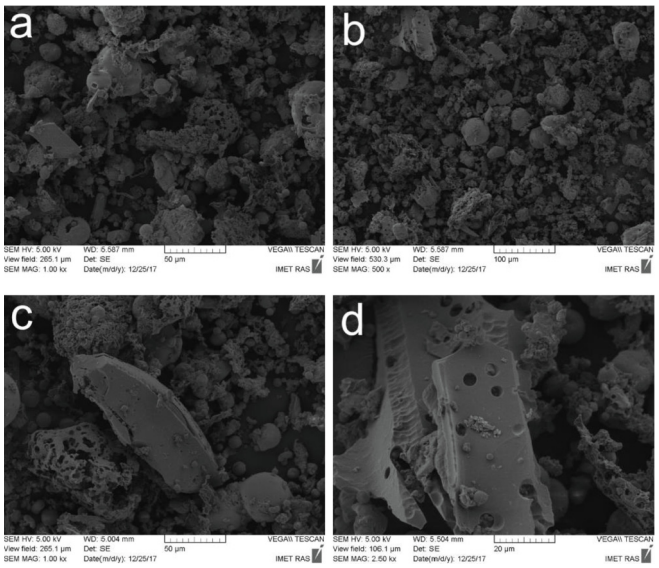

Fig. 8. The SEM micrographs of unburned carbon particles obtained by flotation of the CFA non-magnetic fraction (the collector volume is 5 ml).

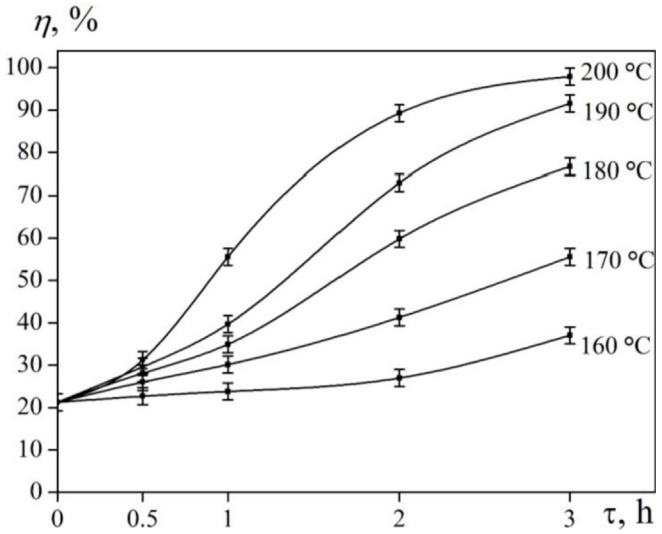

Fig. 9. The effect of the autoclave temperature and exposure time on the Al extraction efficiency (the solid lines are drawn for eye guidance).

Table 5
The average chemical composition [wt. %] of the solid residue after autoclave leaching of CFA by hydrochloric acid at T = 200 °C, S:L = 1:5, τ = 3 h.

Component	SiO_2	Al_2O_3	Fe_2O_3	TiO_2	K_2O	CaO	MgO	MnO	Na_2O	P_2O_5	LOI[a]
Contents	92.05	3.61	0.12	1.67	0.4	0.34	0.07	0.03	0.23	0.46	1.02

[a] LOI – loss on ignition.

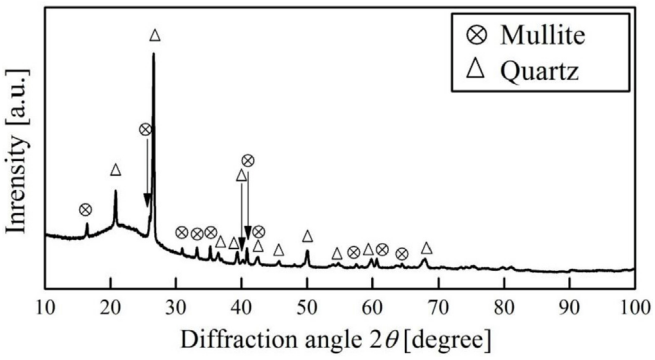

Fig. 10. XRD pattern of the solid residue after autoclave leaching of CFA by HCl at T = 200 °C, S:L = 1:5, τ = 3 h.

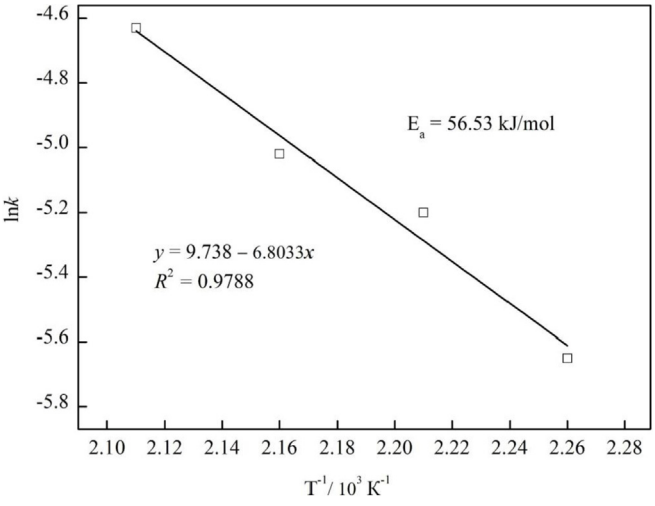

Fig. 11. The logarithm of the reaction rate constant as a function of reciprocal temperature during the autoclave leaching process.

The solid residue that is filtrated after leaching consists mainly of SiO_2 (Table 5) with small amounts of Al_2O_3 and TiO_2. The carbon content is roughly estimated (as LOI) to be around 1 wt %. The XRD analysis shows the presence of quartz and residual mullite (Fig. 10).

This solid residue can further be utilised in ceramic (SiC) manufacturing (Li et al., 2018; Ma et al., 2017) or as an addition to Portland cement to increase its toughness (Reches, 2018; Reches et al., 2018).

Thus, it was found that, using the autoclave HCl leaching process, it is possible to achieve the maximum Al extraction efficiency of ~95% at temperature 200 °C after approximately 3 h. The aluminum chloride solution obtained in the process can be used as a water coagulant, while the solid residue can be utilised in ceramic or cement industries.

3.4. Analysis of the extraction kinetics

The Al extraction process by acid leaching can be described as a reaction rate process (e.g. Valeev et al., 2018) with a thermally activated reaction rate constant. The activation energy for hydrochloric acid leaching of mullite can then be determined from the Arrhenius equation for the reaction rate constant k:

$$k = A \cdot \exp(-E_a / RT) \quad (4)$$

where A is the pre-exponential term; E_a is the activation energy; R is the universal gas constant.

Fig. 11 shows the logarithm of the reaction rate constant as a function of reciprocal temperature constructed on the basis of the experimental data (Fig. 9). The activation energy was determined as a tangent to a linear curve "ln$k$ vs T^{-1}". It can be concluded from the obtained value of E_a (55.5 kJ/mol) that the mullite leaching process is controlled by the corresponding chemical reaction kinetics, not by diffusion, because $E_a > 20$ kJ/mol (Tian et al., 2017).

In order to determine a mechanism of Al extraction by hydrochloric acid leaching of mullite, microstructure of fly ash particles was investigated before and after the autoclave leaching process. Irregular shape particles of 80–90 μm (see Fig. 12, left) were selected as characteristic particles for the non-magnetic fraction. The Al and Si elemental mappings in the particles before and after leaching are also given (Fig. 12, right). It can be seen that all aluminum present on the surface reacted almost completely with hydrochloric acid. The remaining Al is evenly distributed in the bulk and cannot easily be extracted due to surrounding silicon dioxide, which results in a 90–95% Al extraction efficiency. For better Al extraction it might be necessary to reduce the particle size down to 40–50 μm, which is not economically reasonable.

4. Conclusions

1) Combined treatment to utilise the coal fly ash waste collected from the Omsk TPS-4 (Russia) was developed, lab-scale tested and analysed. Three-stage treatment includes magnetic separation of iron-containing fraction, carbon separation by flotation and aluminum extraction by autoclave acid leaching.
2) The magnetite amount in the magnetic fraction after separation increases from 5.3 to 20.2 wt %, while the Al_2O_3 amount in the non-magnetic fraction increases from 24.5 to 27 wt %. The carbon content in the concentrate obtained after flotation using kerosene as the collector reaches ~27 wt %.
3) The effect of the autoclave temperature and exposure time on the aluminum extraction efficiency was investigated for the autoclave hydrochloric acid leaching process. The Al extraction efficiency can reach ~95% at the following optimal process parameters: T = 200 °C, C_{HCl} = 345 g/l, τ = 3 h, S:L = 1:5. The activation energy of the leaching process determined from the experimental data was 56.5 kJ/mol, which value means that the leaching process is controlled by chemical reaction kinetics.
4) The XRD analysis demonstrated that CFA consists mainly of quartz, mullite and magnetite. The microstructure investigation by SEM showed that the magnetite crystals are grown primarily on the surface of alumosilicate spheres. It was also found by SEM that the remaining aluminum (about 5–10%) is evenly distributed in the bulk SiO_2 and its extraction is not economically feasible.

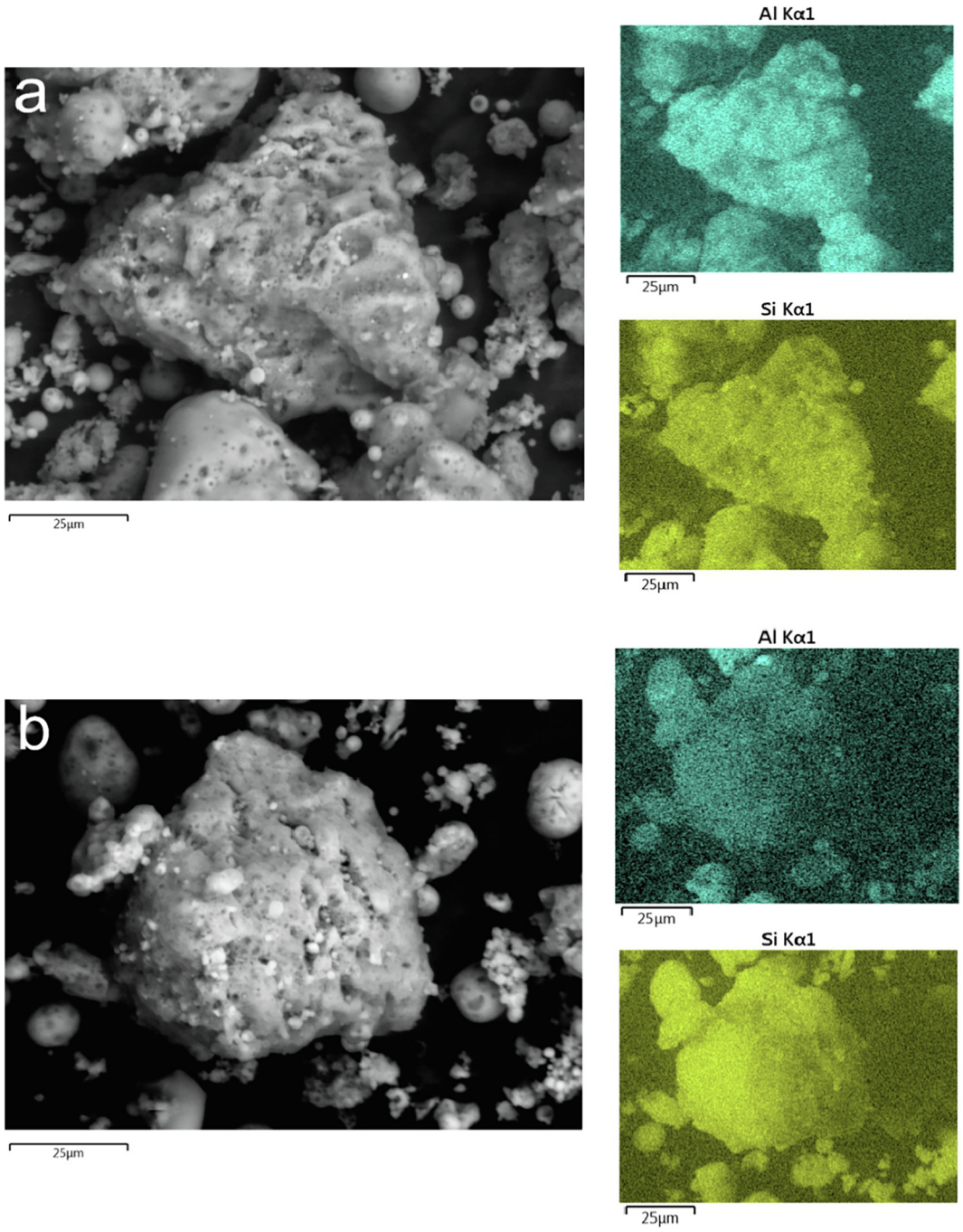

Fig. 12. The SEM micrographs (left) with Al & Si elemental mappings (right) of the non-magnetic CFA samples: (a) an initial particle before autoclave leaching; (b) a particle after autoclave leaching by hydrochloric acid at T = 200 °C, C_{HCl} = 345 g/l, S:L = 1:5 and τ = 3 h.

Conflicts of interest

The authors declare no conflict of interest.

Acknowledgements

The present study was funded by the Russian Science Foundation project No 18-79-00305. The analytical part of the work (X-ray, XRD, SEM, C and S analysis) was carried out in accordance with the Russian Government State Task for Basic Research No. 075-00746-19-00. One of the authors (Kondratiev Alex) was financially supported by the Ministry of Education and Science of the Russian Federation in the framework of the basic part of the state program 'Organisation of the Research Work' for higher educational institutions in 2017–2019 no. 11.7971.2017/6.7.

References

Bartoňová, L., 2015. Unburned carbon from coal combustion ash: an overview. Fuel Process. Technol. 134, 136–158. In: https://doi.org/10.1016/j.fuproc.2015.01.028.

Cheng, F., Cui, L., Miller, J.D., Wang, X., 2012. Aluminum leaching from calcined coal waste using hydrochloric acid solution. Miner. Process. Extr. Metall. Rev. 33, 391–403. https://doi.org/10.1080/08827508.2011.601700.

Dandautiya, R., Singh, A.P., Kundu, S., 2018. Impact assessment of fly ash on ground water quality: an experimental study using batch leaching tests. Waste Manag. Res. 36, 624–634. https://doi.org/10.1177/0734242X18775484.

Dikhanbaev, B., Dikhanbaev, A.B., Sultan, I., Rusowicz, A., 2018. Development of hydrogen-enriched water gas production technology by processing ekibastuz coal with technogenic waste. Arch. Mech. Eng. 65, 221–231. https://doi.org/10.24425/123022.

Ding, J., Ma, S., Shen, S., Xie, Z., Zheng, S., Zhang, Y., 2017. Research and industrialization progress of recovering alumina from fly ash: a concise review. Waste Manag. 60, 375–387. https://doi.org/10.1016/j.wasman.2016.06.009.

Ding, J., Ma, S., Zheng, S., Zhang, Y., Xie, Z., Shen, S., Liu, Z., 2016. Study of extracting alumina from high-alumina PC fly ash by a hydro-chemical process. Hydrometallurgy 161, 58–64. https://doi.org/10.1016/j.hydromet.2016.01.025.

Doucet, F.J., Mohamed, S., Neyt, N., Castleman, B.A., van der Merwe, E.M., 2016. Thermochemical processing of a South African ultrafine coal fly ash using ammonium sulphate as extracting agent for aluminum extraction. Hydrometallurgy 166, 174–184. https://doi.org/10.1016/j.hydromet.2016.07.017.

Flues, M., Sato, I.M., Scapin, M.A., Cotrim, M.E.B., Camargo, I.M.C., 2013. Toxic elements mobility in coal and ashes of Figueira coal power plant. Brazil. Fuel 103, 430–436. https://doi.org/10.1016/j.fuel.2012.09.045.

Gong, B., Tian, C., Xiong, Z., Zhao, Y., Zhang, J., 2016. Mineral changes and trace element releases during extraction of alumina from high aluminum fly ash in Inner Mongolia, China. Int. J. Coal Geol. 166, 96–107. https://doi.org/10.1016/j.coal.2016.07.001.

Guo, Y., Zhao, Q., Yan, K., Cheng, F., Lou, H.H., 2014. Novel process for alumina extraction via the coupling treatment of coal gangue and bauxite red mud. Ind. Eng. Chem. Res. 53, 4518–4521. https://doi.org/10.1021/ie500295t.

Han, G., Yang, S., Peng, W., Huang, Y., Wu, H., Chai, W., Liu, J., 2018. Enhanced recycling and utilization of mullite from coal fly ash with a flotation and metallurgy process. J. Clean. Prod. 178, 804–813. https://doi.org/10.1016/j.jclepro.2018.01.073.

Hower, J.C., Groppo, J.G., Graham, U.M., Ward, C.R., Kostova, I.J., Maroto-Valer, M.M., Dai, S., 2017. Coal-derived unburned carbons in fly ash: a review. Int. J. Coal Geol. 179, 11–27. https://doi.org/10.1016/j.coal.2017.05.007.

Hu, K., Zhao, Q.-L., Chen, W., Tang, F., 2017. Preparation of an aluminum and iron-based coagulant from fly ash for industrial wastewater treatment. Clean. - Soil, Air, Water 45. https://doi.org/10.1002/clen.201600437.

Hu, P., Hou, X., Zhang, J., Li, S., Wu, H., Damø, A.J., Li, H., Wu, Q., Xi, X., 2018. Distribution and occurrence of lithium in high-alumina-coal fly ash. Int. J. Coal Geol. 189, 27–34. https://doi.org/10.1016/j.coal.2018.02.011.

Jiang, Z.Q., Yang, J., Ma, H.W., Wang, L., Ma, X., 2015. Reaction behaviour of Al_2O_3 and SiO_2 in high alumina coal fly ash during alkali hydrothermal process. Trans. Nonferrous Met. Soc. China (English Ed. 25, 2065–2072. https://doi.org/10.1016/S1003-6326(15)63816-X.

Li, F., Guo, Z., Su, G., Guo, C., Sun, G., Zhu, X., 2018. Preparation of SiC from acid-leached coal gangue by carbothermal reduction. Int. J. Appl. Ceram. Technol. 15, 625–632. https://doi.org/10.1111/ijac.12856.

Li, G., Liu, M., Rao, M., Jiang, T., Zhuang, J., Zhang, Y., 2014a. Stepwise extraction of valuable components from red mud based on reductive roasting with sodium salts. J. Hazard Mater. 280, 774–780. https://doi.org/10.1016/j.jhazmat.2014.09.005.

Li, H., Hui, J., Wang, C., Bao, W., Sun, Z., 2014b. Extraction of alumina from coal fly ash by mixed-alkaline hydrothermal method. Hydrometallurgy 147–148, 183–187. https://doi.org/10.1016/J.Hydromet.2014.05.012.

Li, J., Gan, J., Chen, Y., 2011. Acid leaching aluminum from boiler slag - effect of fluoride additives on the aluminum dissolution. Appl. Mech. Mater. 71–78, 688–693. https://doi.org/10.4028/www.scientific.net/AMM.71-78.688.

Li, J., Zhu, J., Qiao, S., Yu, Z., Wang, X., Liu, Y., Meng, X., 2017a. Processing of coal fly ash magnetic spheres for clay water flocculation. Int. J. Miner. Process. 169, 162–167. https://doi.org/10.1016/j.minpro.2017.11.006.

Li, S., Qin, S., Kang, L., Liu, J., Wang, J., Li, Y., 2017b. An efficient approach for lithium and aluminum recovery from coal fly ash by pre-desilication and intensified acid leaching processes. Metals 7, 272. https://doi.org/10.3390/met7070272.

Lin, M., Liu, Y.-Y., Lei, S.-M., Ye, Z., Pei, Z.-Y., Li, B., 2018. High-efficiency extraction of Al from coal-series kaolinite and its kinetics by calcination and pressure acid leaching. Appl. Clay Sci. 161, 215–224. https://doi.org/10.1016/j.clay.2018.04.031.

Liu, D., Fang, L., Guo, Y., Yan, K., Yao, C., Cheng, F., 2018. Effects of calcium oxide and ferric oxide on the process of alumina extraction of coal fly ash activated by sodium carbonate. Hydrometallurgy 179, 149–156. https://doi.org/10.1016/j.hydromet.2018.04.017.

Liu, N., Peng, J., Zhang, L., Wang, S., Huang, S., He, S., 2016. Extraction of aluminum from coal fly ash by alkali activation with microwave heating. J. Residuals Sci. Technol. 13, S181–S187. https://doi.org/10.12783/issn.1544-8053/13/2/S26.

Liu, X.T., Wang, B.D., Yu, G.Z., Xiao, Y.F., Wang, X.W., Zhao, L.J., Sun, Q., 2014. Kinetics study of predesilication reaction for alumina recovery from alumina rich fly ash. Mater. Res. Innovat. 18. S2-541-S2-546. https://doi.org/10.1179/1432891714Z.000000000553.

Lu, M., Chang, Y., Chen, L., 2017. Kinetics of desilification pretreatment from high-aluminum coal fly ash in alkaline medium under pressure. Chem. Res. Chin. Univ. 33, 282–286. https://doi.org/10.1007/s40242-017-6230-y.

Luo, Q., Chen, G., Sun, Y., Ye, Y., Qiao, X., Yu, J., 2013. Dissolution kinetics of aluminum, calcium, and iron from circulating fluidized bed combustion fly ash with hydrochloric acid. Ind. Eng. Chem. Res. 52, 18184–18191. https://doi.org/10.1021/ie4026902.

Ma, B., Ren, X., Yin, Y., Yuan, L., Zhang, Z., Li, Z., Li, G., Zhu, Q., Yu, J., 2017. Effects of processing parameters and rare earths additions on preparation of Al_2O_3-SiC composite powders from coal ash. Ceram. Int. 43, 11830–11837. https://doi.org/10.1016/j.ceramint.2017.05.362.

Reches, Y., 2018. Nanoparticles as concrete additives: review and perspectives. Constr. Build. Mater. 175, 483–495. https://doi.org/10.1016/j.conbuildmat.2018.04.214.

Reches, Y., Thomson, K., Helbing, M., Kosson, D.S., Sanchez, F., 2018. Agglomeration and reactivity of nanoparticles of SiO_2, TiO_2, Al_2O_3, Fe_2O_3, and clays in cement pastes and effects on compressive strength at ambient and elevated temperatures. Constr. Build. Mater. 167, 860–873. https://doi.org/10.1016/j.conbuildmat.2018.02.032.

Ruhl, L., Vengosh, A., Dwyer, G.S., Hsu-Kim, H., Deonarine, A., Bergin, M., Kravchenko, J., 2009. Survey of the potential environmental and health impacts in the immediate aftermath of the coal ash spill in Kingston, Tennessee. Environ. Sci. Technol. 43, 6326–6333. https://doi.org/10.1021/es900714p.

Ryabov, Y.V., Delitsyn, L.M., Ezhova, N.N., 2016. Flotation recovery of carbon from fly ash of coal-fired power plants using mix of kerosene with gasoil. Obogashchenie Rud 48–54. https://doi.org/10.17580/or.2016.05.09.

Ryabov, Y.V., Delitsyn, L.M., Ezhova, N.N., Lavrinenko, A.A., 2018. PAV-2 conditioning agent application efficiency in flotation of unburned carbon from coal-fired power plants fly ash. Obogashchenie Rud 43–49. https://doi.org/10.17580/or.2018.01.08.

Sahoo, P.K., Kim, K., Powell, M.A., Equeenuddin, S.M., 2016. Recovery of metals and other beneficial products from coal fly ash: a sustainable approach for fly ash management. Int. J. Coal Sci. Technol. 3, 267–283. https://doi.org/10.1007/s40789-016-0141-2.

Sangita, S., Nayak, N., Panda, C.R., 2017. Extraction of aluminum as aluminum sulphate from thermal power plant fly ashes. Trans. Nonferrous Met. Soc. China (English Ed. 27. https://doi.org/10.1016/S1003-6326(17)60231-0, 2082–2089.

Schins, R.P.F., Borm, P.J.A., 1999. Mechanisms and mediators in coal dust induced toxicity: a review. Ann. Occup. Hyg. 43, 7–33. https://doi.org/10.1016/S0003-4878(98)00069-6.

Singh, R., Singh, L., Singh, S.V., 2015. Beneficiation of iron and aluminum oxides from fly ash at lab scale. Int. J. Miner. Process. 145, 32–37. https://doi.org/10.1016/j.minpro.2015.08.001.

Sirotyuk, V.V., Lunev, A.A., 2017. Strength and deformation characteristics of ash and slag mixture. Mag. Civ. Eng. 74, 1–14. https://doi.org/10.18720/MCE.74.1.

Sun, L., Luo, K., Fan, J., Lu, H., 2017. Experimental study of extracting alumina from coal fly ash using fluidized beds at high temperature. Fuel 199, 22–27. https://doi.org/10.1016/j.fuel.2017.02.073.

Sun, Z., Li, H., Bao, W., Wang, C., 2016. Mineral phase transition of desilicated high alumina fly ash with alumina extraction in mixed alkali solution. Int. J. Miner. Process. 153, 109–117. https://doi.org/10.1016/j.minpro.2016.05.004.

Tanvar, H., Chauhan, S., Dhawan, N., 2018. Extraction of aluminum values from fly ash. Mater. Today-Proceedings 5, 17055–17063. https://doi.org/10.1016/j.matpr.2018.04.112.

Tian, L., Liu, Y., Zhang, T.A., Lv, G.Z., Zhou, S., Zhang, G.Q., 2017. Kinetics of indium dissolution from marmatite with high indium content in pressure acid leaching. Rare Met. 36, 69–76. https://doi.org/10.1007/s12598-016-0762-z.

Tripathy, A.K., Sarangi, C.K., Tripathy, B.C., Sanjay, K., Bhattacharya, I.N., Mahapatra, B.K., Behera, P.K., Satpathy, B.K., 2015. Aluminum recovery from NALCO fly ash by acid digestion in the presence of fluoride ion. Int. J. Miner. Process. 138, 44–48. https://doi.org/10.1016/j.minpro.2015.03.010.

Valeev, D., Mikhailova, A., Atmadzhidi, A., 2018. Kinetics of iron extraction from coal fly ash by hydrochloric acid leaching. Metals 8. https://doi.org/10.3390/met8070533.

Valentim, B., Białecka, B., Gonçalves, P.A., Guedes, A., Guimarães, R., Cruceru, M., Całus-Moszko, J., Popescu, L.G., Predeanu, G., Santos, A.C., 2018. Undifferentiated inorganics in coal fly ash and bottom ash: calcispheres, magnesiacalcispheres, and magnesiaspheres. Minerals 8. https://doi.org/10.3390/min8040140.

van der Merwe, E.M., Gray, C.L., Castleman, B.A., Mohamed, S., Kruger, R.A., Doucet, F.J., 2017. Ammonium sulphate and/or ammonium bisulphate as extracting agents for the recovery of aluminum from ultrafine coal fly ash. Hydrometallurgy 171, 185–190. https://doi.org/10.1016/j.hydromet.2017.05.015.

Vasilyev, A.M., Kuskov, V.B., 2018. Specific features of the concentration process for fine-grained materials in a short-cone hydrocyclone. Obogashchenie Rud 30–34. https://doi.org/10.17580/or.2018.02.06.

Wang, R., Zhai, Y., Ning, Z., Ma, P., 2014. Kinetics of SiO_2 leaching from Al_2O_3 extracted slag of fly ash with sodium hydroxide solution. Trans. Nonferrous Metals Soc. China 24, 1928–1936. https://doi.org/10.1016/S1003-6326(14)63273-8.

Wei, C., Cheng, S., Zhu, F., Tan, X., Li, W., Zhang, P., Miao, S., 2018. Digesting high-aluminum coal fly ash with concentrated sulfuric acid at high temperatures. Hydrometallurgy 180, 41–48. https://doi.org/10.1016/j.hydromet.2018.07.004.

Wu, C.-Y., Yu, H.-F., Zhang, H.-F., 2012. Extraction of aluminum by pressure acid-leaching method from coal fly ash. Trans. Nonferrous Met. Soc. China (English Ed. 22, 2282–2288. https://doi.org/10.1016/S1003-6326(11)61461-1.

Wu, Y., Li, L., Li, M., 2014. Effect of pressure on alumina extraction from low-grade bauxite by acid-leaching method. In: TMS Light Metals. Minerals, Metals and Materials Society, San Diego, CA, pp. 121–123.

Xiao, J., Zhang, L., Yuan, J., Yao, Z., Tang, L., Wang, Z., Zhang, Z., 2018. Co-utilization of spent pot-lining and coal gangue by hydrothermal acid-leaching method to prepare silicon carbide powder. J. Clean. Prod. 204, 848–860. https://doi.org/10.1016/j.jclepro.2018.08.331.

Yan, K., Guo, Y., Liu, D., Ma, Z., Cheng, F., 2018. Thermal decomposition and transformation mechanism of mullite with the action of sodium carbonate. J. Solid State Chem. 265, 326–331. https://doi.org/10.1016/j.jssc.2018.06.014.

Yan, L., Wang, Y., Li, J., Shen, H., Zhang, C., Qu, T., 2016. Preparation of polymeric

aluminum ferric chloride (PAFC) coagulant from fly ash for the treatment of coal-washing wastewater. Desalin. Water Treat. 57, 18260–18274. https://doi.org/10.1080/19443994.2015.1089420.
Yang, L., Li, D., Zhang, H., Yan, X., 2018. Flotation kinetics of the removal of unburned carbon from coal fly ash. Energy Sources, Part A Recover. Util. Environ. Eff. 40, 1781–1787. https://doi.org/10.1080/15567036.2018.1486914.
Zhang, Z.-Y., Qiao, X.-C., Yu, J.-G., 2015. Aluminum release from microwave-assisted reaction of coal fly ash with calcium carbonate. Fuel Process. Technol. 134, 303–309. In: https://doi.org/10.1016/j.fuproc.2014.12.050.